Available online at www.sciencedirect.com
SCIENCE DIRECT®
Journal of Solid State Chemistry 177 (2004) 1197–1212
JOURNAL OF SOLID STATE CHEMISTRY
http://elsevier.com/locate/jssc

Variation of the crystal structures of incommensurate LT′-$Ni_{1+\delta}Sn$ ($\delta = 0.35, 0.38, 0.41$) and commensurate LT-$Ni_{1+\delta}Sn$ ($\delta = 0.47, 0.50$) with composition and annealing temperature

A. Leineweber*

Max Planck Institute for Metals Research, Heisenbergstraße 3, 70569 Stuttgart, Germany

Received 9 June 2003; received in revised form 12 October 2003; accepted 29 October 2003

Abstract

The variation of the crystal structures of two $Ni_{1+\delta}Sn$ phases (ordered NiAs/Ni_2In-type structures) as a function of the annealing temperature and composition was studied on the basis of X-ray powder patterns evaluated by Rietveld refinement. In both phases—incommensurate LT′ ($\delta = 0.35, 0.38, 0.41$; *Cmcm*($\alpha$00)0*s*0, $\alpha < 1/2$) and commensurate LT ($\delta = 0.47, 0.50$; *Pbnm*)—the occupation modulations of Ni atoms in these phases cause strong displacements of all atoms from their ideal sites. The artificial description of the LT phase (for which 'conventional' structural parameters have been reported previously) as a commensurately modulated structure (*Pbnm* section of *Cmcm*(α00)0*s*0 with $\alpha = 1/2$) allows a common analysis of the concentration and annealing-temperature-dependent modulation parameters of both phases, which reveals their close structural similarities. This confirms that the LT phase can be regarded as a commensurate special case (lock-in phase) of the LT′ phase.

Keywords: Order–disorder phase transitions; Modulated structures; Incommensurate structures; Rietveld refinement

1. Introduction

The phase field 'Ni_3Sn_2' of the system Ni–Sn comprises a range of compositions according to $Ni_{1+\delta}Sn$ with ca. $0.35 < \delta < 0.67$ (maximum extent according to Ref. [1]). The crystal structures of the different phases occurring in this field belong to the large group of NiAs/Ni_2In-type structures $T_{1+\delta}B$ with *T*: transition metal and *B*: main group metal [2,3]. For the particular system of interest, 'Ni(1)Sn' forms a NiAs-type arrangement (Ni(1) in the octahedral sites of an hcp-type arrangement of Sn; the *c*/*a* axial ratio is reduced—with respect to 1.633 for ideal hcp—to about 1.26–1.27) with Ni(2) on trigonal–bipyramidal sites formed by five Sn atoms giving the formula Ni(1)-$Ni(2)_\delta Sn$ or, in short, $Ni_{1+\delta}Sn$.

The high-temperature (HT) phase, which exists for the whole range of δ, shows no long-range order of Ni(2) on the trigonal-bipyramidal sites. Consequently, its symmetry is $P6_3/mmc$ with Sn on the 2*c* Wyckoff-site (1/3, 2/3, 1/4), Ni(1) on 2*a* (0, 0, 0) and Ni(2) on 2*d* (1/3, 2/3, 3/4) with an occupancy of δ (cf. Fig. 1).

The HT phase is stable above a composition-dependent ordering temperature which has a maximum of 750 K at $\delta \approx 0.45-0.50$ [4], but the HT phase can readily be retained at ambient temperatures by water quenching [5].

Upon annealing at temperatures below the ordering temperature, different low-temperature phases can be generated. For $\delta > 0.55$ ordering has not been reported before, however, recent investigations show that an ordered LT″ phase exists in this range (A. Leineweber, unpublished). For lower Ni contents around the 'stoichiometric' composition $Ni_{1.50}Sn$ (Ni_3Sn_2) the LT phase occurs, which was characterized by X-ray diffraction applying a twinned crystal specimen [6]. The superlattice is $a_{LT} \approx 2a_{HT}$, $b_{LT} \approx 3^{1/2}a_{HT}$ and $c_{LT} \approx c_{HT}$ with symmetry *Pbnm* (the *Pnam* setting was used in the original work [6], the standard setting would be *Pnma*; Fig. 2). The phase transition LT→HT was characterized as of first order [4].

The LT phase occurs only in the range $0.45 < \delta < 0.55$ [7]. At variance with previous results [4], an

*Fax: +49-711-689 3312.
E-mail address: a.leineweber@mf.mpg.de.

0022-4596/$ - see front matter © 2003 Elsevier Inc. All rights reserved.
doi:10.1016/j.jssc.2003.10.028

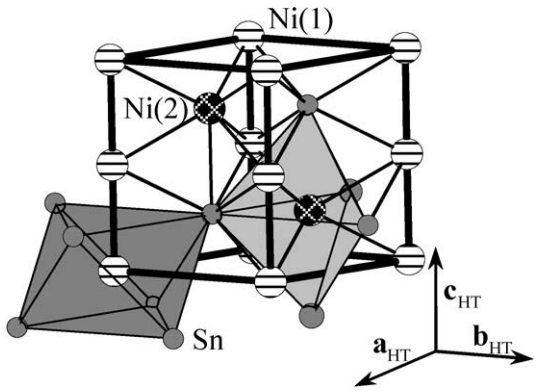

Fig. 1. HT–$Ni_{1+\delta}Sn$ (i.e., Ni(1)Ni(2)$_\delta$Sn): One unit cell extended with additional Sn atoms in order to illustrate the octahedral coordination of Ni(1) and the trigonal-bipyramidal one of Ni(2) (occupancy: δ) by Sn, respectively.

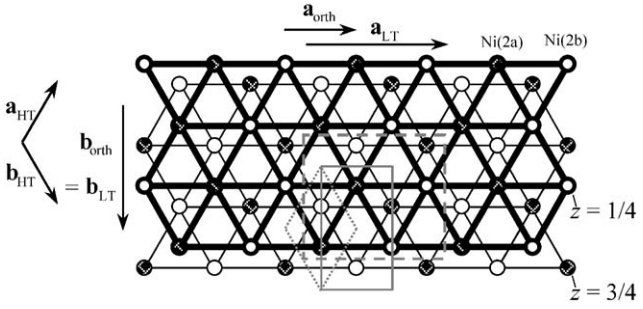

Fig. 2. Occupational ordering pattern in LT-$Ni_{1+\delta}Sn$ (ideal composition $Ni_{1.50}Sn$ i.e., 'Ni_3Sn_2') showing only the Ni(2) sites, which form by themselves an *hcp*-like arrangement. The splitting into (ideally fully) occupied Ni(2a) and not-occupied Ni(2b) sites leads to symmetry reduction to *Pbnm*. The relation between the unit cells of the hexagonal HT phase, of the orthorhombic average structure (which is the same for the LT- and LT′ phases) and of the 'conventionally' described *Pbnm* LT-superstructure is indicated.

incommensurately ordered phase occurs for $0.35<\delta<0.45$ which has been labelled the LT′ phase [7]. The LT′ phase has a *C*-centered orthorhombic average structure with $a_{orth}\approx a_{HT}$, $b_{orth}\approx 3^{1/2}a_{HT}$, $c_{orth}\approx c_{HT}$ (cf. Table 1) and a modulation vector $\mathbf{q}=\alpha\mathbf{a}^*_{orth}$ with $\alpha\approx 0.493$ for $\delta=0.44$ and $\alpha\approx 0.428$ for $\delta=0.35$. According to systematic extictions the (3+1)-dimensional superspace group $Cmcm(\alpha 00)0s0$ was obtained.

In Ref. [7] no structure refinements for the LT′ phase were performed. However, correspondences between the diffraction patterns of the LT and the LT′ phase suggested a qualitative model for the ordered distribution of the Ni(2) atoms. According to that the LT phase was regarded as a commensurate *lock-in* phase of the LT′ phase with the same *C*-centered orthorhombic average structure and a modulation vector $\mathbf{q}=\mathbf{a}^*_{orth}/2$ (i.e., $\alpha=1/2$) giving the above-mentioned *Pbnm* superstructure cell of the LT phase [7].

In this paper, the concentration and annealing-temperature-dependent crystal structure of the LT′ phase is quantitatively evaluated by Rietveld refinement on the basis of X-ray powder diffraction patterns. Furthermore, the crystal structure of the LT phase was re-evaluated in the same way in order to relate the crystal structures of the LT′ and the LT phase with each other.

2. Experimental

2.1. Preparation and heat treatment

$Ni_{1+\delta}Sn$ alloys (same as used in Ref. [7]; $\delta=0.352$, 0.381, 0.410, 0.469 0.500; in the following only two digits will be used to label the different samples) were prepared from Ni sheets (1 mm thickness, 99.98 mass%, Goodfellow) and Sn pieces (bars, Heraeus 99.999 mass%). The batch sizes were about 32–35 g. The starting materials were melted by induction heating and cast into water-cooled cylindrical forms of diameter 8 mm and length 50 mm. The mass of the cast ingots confirmed that there was no significant loss of mass during alloy production.

The top and bottom parts of the cast cylinders were removed. The remaining material was sealed in quartz tubes and subjected to a homogenization treatment of 3 d at 473 K[1] and 3 d at 1023 K followed by water quenching by crushing the quartz tube. Thereby, a homogeneous bulk specimen of the HT phase was obtained. According to Ref. [7], results from chemical analysis of the alloys agreed well with the weighted amounts of Ni and Sn used for melting the alloys.

Deviating now from the preparation procedures applied in Ref. [7], starting from the HT phase bulk specimen powder batches (approximately 1 g) were prepared by grinding in a mortar. This produced moderate but significant diffraction line broadening caused by residual micro-stresses, which could be virtually removed completely by a heat treatment of 15 min at 1023 K followed by quenching by putting the quartz ampoule into water.

In order to obtain LT and LT′ phase specimen, the stress-relieved powder batches were annealed for 5 d at 673 K and quenched. Furthermore, a part of the thus treated powder batch was subsequently annealed for 2 d at 573 K and 2 d at 473 K followed by quenching. Thereby, two powder batches quenched from 673 K as well as from 473 K were obtained, which were used to collect the powder diffraction data for Rietveld refinement. Furthermore, a small amount of the batch quenched from 473 K was annealed for additional

[1] The treatment at 473 K was chosen in order to remove Sn-rich inhomogeneities of the cast material, avoiding their melting.

Table 1
Superspace group description of incommensurate LT′- (*Cmcm*(α00)0*s*0) and commensurately modulated LT–$Ni_{1+\delta}Sn$ (*Cmcm*(α00)0*s*0 with terms for the *Pbnm* section)

Average structure of the LT and LT′ phases: *Cmcm*, $a_{orth} \approx a_{HT}$, $b_{orth} \approx 3^{1/2} a_{HT}$, $c_{orth} \approx c_{HT}$				
Atom M	x^M	y^M	z^M	Occupancy
Sn	0	y_{av}^{Sn}	1/4	1
Ni(1)	0	0	0	1
Ni(2)	0	$y_{av}^{Ni(2)}$	1/4	δ

Final coordinates and occupancies of the atoms as resulting from the average structure and the modulation functions $u^M(x_4)$ and $p^M(x_4)$[a]

Sn

$x^{Sn} = 0 + u_x^{Ni(2)}(x_4) = 0 + u_{x,c,1}^{Sn} \cos 2\pi x_4 + u_{x,s,2}^{Sn} \sin 4\pi x_4 \{+u_{x,c,3}^{Sn} \cos 6\pi x_4\}$

$y^{Sn} = y_{av}^{Sn} + u_y^{Sn}(x_4) = y_{av}^{Sn} + u_{y,s,1}^{Sn} \sin 2\pi x_4 \{+u_{y,c,2}^{Sn} \cos 4\pi x_4 + u_{y,s,3}^{Sn} \sin 6\pi x_4\}$

$z^{Sn} = 1/4$

$occ^{Sn} = 1$

Ni(1)

$x^{Ni(1)} = 0 + u_x^{Ni(1)}(x_4) = u_{x,s,2}^{Ni(1)} \sin 4\pi x_4$

$y^{Ni(1)} = 0 + u_y^{Ni(1)}(x_4) = u_{y,s,1}^{Ni(1)} \sin 2\pi x_4$

$z^{Ni(1)} = 0 + u_y^{Ni(1)}(x_4) = u_{z,s,1}^{Ni(1)} \sin 2\pi x_4$

$occ^{Ni(1)} = 1$

Ni(2)

$x^{Ni(2)} = 0 + u_x^{Ni(2)}(x_4) = 0 + u_{x,c,1}^{Ni(2)} \cos 2\pi x_4 + u_{x,s,2}^{Ni(2)} \sin 4\pi x_4$

$y^{Ni(2)} = y_{av}^{Ni(2)} + u_y^{Ni(2)}(x_4) = y_{av}^{Ni(2)} + u_{y,s,1}^{Ni(2)} \sin 2\pi x_4 \{+u_{y,c,2}^{Ni(2)} \cos 4\pi x_4\}$

$z^{Ni(2)} = 1/4$

$occ^{Ni(2)} = \delta + p^{Ni(2)}(x_4) = \delta + p_{s,1}^{Ni(2)} \sin 2\pi x_4 \{+p_{c,2}^{Ni(2)} \cos 4\pi x_4\}$

[a] Terms in { } are not relevant for the commensurate LT case. For the LT′ phase only those terms are listed, which are relevant for discussion. However, in the actual final refinements, not all terms were used (see Section 3 and Table 3).

15 min at 1023 K and quenched. These samples were used for the X-ray studies on the HT phase.

For the heat treatments it was assumed—and the results make it likely—that by quenching the state of order which corresponds to the last annealing temperature is successfully retained at ambient temperatures.

2.2. X-ray diffraction

Accurate cell parameters for the powder samples quenched from 1023, 673 and 473 K were determined on the basis of diffractograms taken on a Philips X'Pert MPD diffractometer equipped with a primary beam monochromator selecting Cu $K\alpha 1$ radiation. A thin layer of $Ni_{1+\delta}Sn$ powder with Ge as internal standard (99.9999 wt%, Johnson Matthey, $a_{Ge} = 5.6574$ Å [8]) on a (510) cut Si wafer was examined in the range $26° < 2\theta < 68°$, where 2θ is the diffraction angle. Reflection positions were determined in this range using the programme ProFit [9]. The 2θ scale was calibrated using the Ge reflections. The resulting positions of the $Ni_{1+\delta}Sn$ reflections were used as input for a least-square fitting procedure (ASIN [10]) yielding the cell parameters.

For the Rietveld refinements, of all samples quenched from 673 to 473 K diffraction patterns were recorded on a Philips X'Pert MPD diffractometer with $\theta-\theta$ arrangement and Bragg–Brentano geometry, equipped with Cu $K\alpha$ radiation (1.54056 and 1.54439 Å) and a graphite monochromator in the diffracted beam. The samples consisted of 1 mm back-loaded powder, diameter 10 mm. Continuous scan data were collected within a range of $2\theta = 10-130°$.

2.3. Rietveld refinement and structural models for LT- and LT′-$Ni_{1+\delta}Sn$ phases

Rietveld refinement for LT- and LT′-$Ni_{1+\delta}Sn$ was performed using the JANA2000 package [11]. The background was described using Legendre polynoms with eight coefficients. Reflection profiles were fitted with pseudo-Voigt-type functions [12]. Only the Gaussian V and the Lorentzian X and Y parameters [12] as well as zero-point shifts were refined.

All structural refinements were done keeping the occupancy of all Ni(2) sites to the balanced quantities of Sn and Ni, δ. Always only two isotropic atomic displacement parameters were considered, one for Ni and one for Sn.

Table 2
Results from cell parameter measurements and Rietveld refinement (first part) for HT-, LT- and LT′-$Ni_{1+\delta}Sn$

Sample	T_{ann} (K)[a]	From cell parameter determination				From Rietveld refinement			
		a_{HT}, c_{HT} or a_{orth}, b_{orth}, c_{orth} (Å) against Ge[b]	V[c] (Å^3)	c/a and $(c/a)_{eff}$[d] $\Delta c/a$[e]	Orth. dist. $(b_{orth}/3^{1/2}a_{orth}) - 1$	a_{orth}, b_{orth}, c_{orth} (Å) from Rietveld[b]	α as to $\mathbf{q} = \alpha\mathbf{a}^*_{orth}$	R_P/R_{wP}	R_{Bragg}[f]
HT-$Ni_{1.50}Sn$	1023	4.1050(1) 5.1797(1)	75.59	1.2618	0	—	—	—	—
LT-$Ni_{1.50}Sn$	673	4.0758(2) 7.1238(3) 5.1953(2)	75.42	1.2689 0.0071	0.0091	4.07625(3) 7.12434(6) 5.19513(4)	1/2	12.2/17.9	3.7/5.2
LT-$Ni_{1.50}Sn$	473	4.0738(1) 7.1248(2) 5.1957(1)	75.40	1.2692 0.0074	0.0098	4.07393(4) 7.12485(6) 5.19609(4)	1/2	12.8/18.4	4.3/5.0
HT-$Ni_{1.47}Sn$	1023	4.0988(2) 5.1742(2)	75.28	1.2624	0	—	—		
LT-$Ni_{1.47}Sn$	673	4.0696(1) 7.1131(2) 5.1883(2)	75.09	1.2691 0.0067	0.0091	4.07000(3) 7.11323(6) 5.18842(5)	1/2	13.3/19.0	4.5/5.6
LT-$Ni_{1.47}Sn$	473	4.0680(1) 7.1141(2) 5.1890(1)	75.09	1.2694 0.0070	0.0097	4.06844(3) 7.11406(6) 5.18936(4)	1/2	13.1/18.4	4.1/4.5
HT-$Ni_{1.41}Sn$	1023	4.0831(3) 5.1588(3)	74.48	1.2635	0	—	—	—	—
LT′-$Ni_{1.41}Sn$	673	4.0604(1) 7.0869(2) 5.1679(2)	74.35	1.2679 0.0044	0.0077	4.06064(4) 7.08697(6) 5.16825(4)	0.45618(3)	13.3/18.7	3.7/6.6

LT′-$Ni_{1.41}Sn$	473	4.0551(1) 7.0895(2) 5.1705(1)	74.32	1.2691 0.0056	0.0094	4.05521(4) 7.08975(6) 5.17129(4)	0.45598(3)	14.0/19.1	3.8/5.6
HT-$Ni_{1.38}Sn$	1023	4.0766(1) 5.1524(1)	74.15	1.2639	0	—	—	—	—
LT′-$Ni_{1.38}Sn$	673	4.0552(2) 7.0752(2) 5.1605(1)	74.03	1.2679 0.0040	0.0073	4.05500(4) 7.07539(6) 5.16047(4)	0.43775(3)	13.4/18.5	3.8/6.6
LT′-$Ni_{1.38}Sn$	473	4.0483(1) 7.0795(2) 5.1644(1)	74.01	1.2696 0.0057	0.0097	4.04838(4) 7.07959(6) 5.16465(5)	0.43780(3)	13.4/19.3	3.9/6.2
HT-$Ni_{1.35}Sn$	1023	4.0695(2) 5.1447(2)	73.79	1.2642	0	—	—	—	—
LT′-$Ni_{1.35}Sn$	673	4.0517(1) 7.0618(1) 5.1520(1)	73.71	1.2676 0.0034	0.0063	4.05209(4) 7.06225(7) 5.15232(5)	0.42817(4)	13.4/18.7	3.9/7.7
LT′-$Ni_{1.35}Sn$	473	4.0413(2) 7.0684(2) 5.1578(2)	73.67	1.2701 0.0059	0.0096	4.04101(4) 7.06768(7) 5.15782(5)	0.42703(3)	13.9/19.4	3.9/5.9

[a] Final annealing temperature before quenching.

[b] Note, that for the LT/ LT′ phases the orthorhombic cell parameters refer to the average structure. For the commensurate LT phase, the 'conventional' cell parameters referring to the *Pbnm* superstructure are $a_{LT} = 2a_{orth}$, $b_{LT} = 3^{1/2}b_{orth}$, $c_{LT} = c_{orth}$ (see Table 4).

[c] Corresponds to the volume of a HT-type unit cell, which means $V_{orth}/2$ for the LT/LT′ phase cases.

[d] For the HT phase c_{HT}/a_{HT}, for LT/LT′ $(c/a)_{eff} = c_{orth}/(a_{orth}\cdot b_{orth}/3^{1/2})^{1/2}$.

[e] $\Delta c/a = (c/a)_{eff} - c_{HT}/a_{HT}$ (1023 K).

[f] For LT and LT′: *R* (all main reflections), *R* (all first-order satellites). For the LT′ phase the second-order reflections were also considered, however, were not observed by visual inspection of the diffraction data. Therefore, the corresponding R_{Bragg} values are meaningless and are not listed here.

The modulated structure models for the LT and LT′ phases are both based on the same orthorhombic average structure having *Cmcm* symmetry and on a Fourier series description of the modulation functions of the different structural parameters (cf. Table 1). The modulation functions have a similar shape as those listed in Ref. [13]. x_4 takes the role of the fourth fractional coordinate of the $(3+1)$-dimensional superspace with $x_4 = t + \mathbf{q}\cdot(\mathbf{l}+\mathbf{r}_0)$ with $\mathbf{l}$ being a vector of the average lattice, $\mathbf{r}_0$ the coordinate of the atom in the average structure, and t determining the position, at which the hyperplane corresponding to the three-dimensional structure intersects the $(3+1)$-dimensional superspace, which is only of special structural relevance for the commensurate case.

In the powder diffraction data of the LT′ phase samples, only first-order satellites were observed. Nevertheless, during the Rietveld refinement, also the calculated intensities for satellites of second order were considered in order to impose—at least—that their intensity is negligible within the range of noise of the intensity data. Due to the limited information provided by the powder diffraction data in terms of satellite-reflection order, it is to be expected that for the different modulation functions only Fourier coefficients up to a limited order can be determined, although, for an incommensurate phase an infinite number of terms may be required for the description of the 'true' structure. The number of refined orders and their relevance to the resulting structure model are discussed in Section 3.

Especially incommensurate occupational modulations are often inadequately described by a Fourier series with a limited number of terms. A frequently used alternative is a *Crenel*-type function [14]. This can be postulated as a 'maximum ordered reference state' of an incommensurate structure with a specific value of α and a composition δ: On the x_4 scale for a length of δ the occupancy is 1 and for a length of $(1-\delta)$ it is 0. The corresponding Fourier series for a *Crenel*-type occupational modulation function for a given $\alpha^{\mathbf{a}*}_{\mathrm{worth}}$ is

$$\mathrm{occ}^{\mathrm{Ni(2)}}(x_4) = \delta + \frac{2}{\pi}\sin\pi\delta\sin 2\pi x_4 + \frac{2}{2\pi}\sin 2\pi\delta\cos 4\pi x_4 + \frac{2}{3\pi}\sin 3\pi\delta\cos 6\pi x_4. \quad (1)$$

Such a *Crenel*-type description for the occupational modulation of Ni(2) in the incommensurate LT′ phase was checked by Rietveld refinement in comparison with the Fourier approach outlined in Table 1.

The LT phase is described here as a commensurately modulated structure with $\mathbf{q} = \mathbf{a}^*_{\mathrm{orth}}/2$, which is fully equivalent to a description as a 'conventional' superstructure with $a_{\mathrm{LT}} = 2a_{\mathrm{orth}}$, $b_{\mathrm{LT}} = b_{\mathrm{orth}}$, $c_{\mathrm{LT}} = c_{\mathrm{orth}}$ [15]. For the modulated structure description, different values of t correspond to different superstructures which are, in principle, distinguishable from their diffraction patterns [16]. It should be likely that this can be achieved here, since with respect to the HT phase, the unit cell volume of the LT phase is only quadrupled, i.e., the LT phase can be regarded as a short-period modulated structure [14,17]. Analogous to the considerations made in Refs. [13,18], the unequivalent structures have the space group symmetries *Pbnm* for $t = 1/8 + n/4$ ($n \in \mathbb{Z}$), *Pmnm* for $t = 0 + n/4$ ($n \in \mathbb{Z}$) and $P2_1nm$ for all other values of t. *Pbnm* corresponds to the previously reported structure for LT-$Ni_{1+\delta}Sn$ [4,6]. Separate Rietveld refinements were made for different values of t.

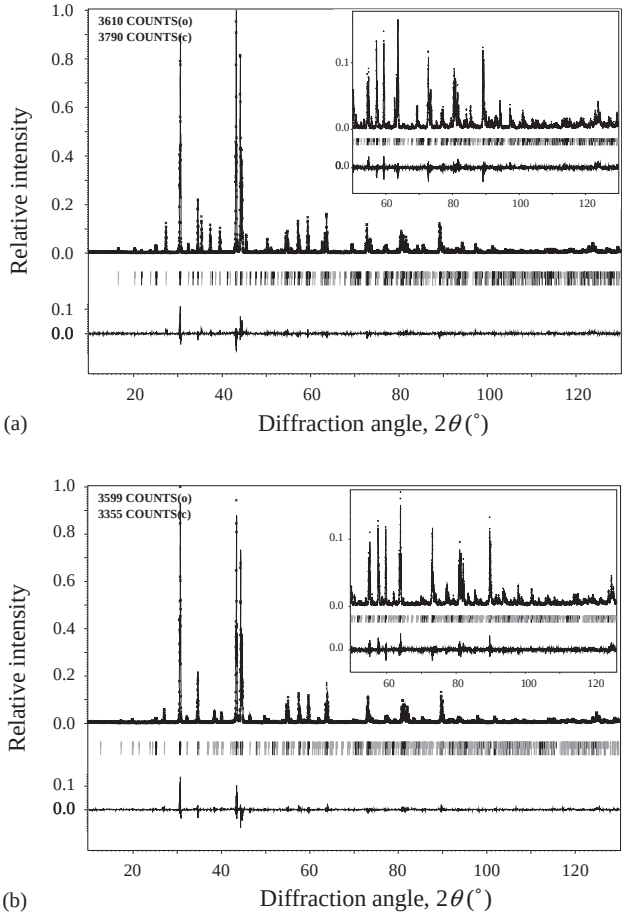

Fig. 3. Rietveld fits of X-ray diffraction data on the samples LT-$Ni_{1.50}Sn$ (a) and LT′-$Ni_{1.41}Sn$ (b) (both quenched from 473 K): Observed data points, fitted and difference curves and reflection markers, respectively. Satellite/superstructure reflections are indicated in grey.

3. Experimental results

As expected, the samples quenched from 1023 K consisted of HT phase, whereas those quenched from 673 or 473 K were of LT′ ($\delta = 0.35$, 0.38, 0.41) or LT phase ($\delta = 0.47$, 0.50). The unit cell parameters as

Table 3
Results from Rietveld refinement (second part) of LT- and LT′-$Ni_{1+\delta}Sn$ quenched from 673 or 473 K, respectively: atomic displacement parameters, amplitudes of atomic modulation functions (displacive, u^M, and occupational, $p^{Ni(2)}$, according to Table 1)

Sample	T_{ann} (K)[a]	U_{Ni}, U_{Sn} (Å^2)	$-u^{Sn}_{x,c,1}$, $-u^{Sn}_{x,s,2}$, $u^{Sn}_{x,c,3}$ [b]	y^{Sn}_{av}, $-u^{Sn}_{y,s,1}$, $u^{Sn}_{y,c,2}$ [b], $u^{Sn}_{y,s,3}$ [b]	$u^{Ni(1)}_{x,s,2}$	$-u^{Ni(1)}_{y,s,1}$	$u^{Ni(1)}_{z,s,1}$	$p^{Ni(2)}_{s,1}$	$u^{Ni(2)}_{x,c,1}$	$y^{Ni(2)}_{av}$
LT-$Ni_{1.50}Sn$	673	0.0146(4) 0.0126(3)	0.0639(3) 0.0126(3) —	0.3292(1) 0.0267(2) — —	0.0001(7)	0.0210(4)	0.0049(6)	0.693(5)	0.004(1)	0.6589(5)
LT-$Ni_{1.50}Sn$	473	0.0133(4) 0.0113(3)	0.0660(3) 0.0129(3) —	0.3289(1) 0.0274(2) — —	0.0002(8)	0.0225(4)	0.0065(6)	0.715(5)	0.006(1)	0.6589(4)
LT-$Ni_{1.47}Sn$	673	0.0126(4) 0.0116(3)	0.0609(3) 0.0119(3) —	0.3295(2) 0.0255(2) — —	0.0022(8)	0.0210(4)	0.0066(6)	0.675(5)	0.003(1)	0.6591(5)
LT-$Ni_{1.47}Sn$	473	0.0130(4) 0.0119(2)	0.0623(3) 0.0128(3)	0.3293(2) 0.0257(2) — —	0.0009(8)	0.0208(4)	0.0060(6)	0.666(5)	0.010(1)	0.6596(5)
LT′-$Ni_{1.41}Sn$	673	0.0125(5) 0.0137(3)	0.0464(4) 0.0151(6) 0.023(1)	0.3311(2) 0.0198(2) 0.0044(4) 0.002(1)	0.006(2)	0.0186(5)	0.0066(7)	0.498(5)	0.002(2)	0.6603(6)
LT′-$Ni_{1.41}Sn$	473	0.0127(5) 0.0127(4)	0.0495(4) 0.0172(6) 0.026(1)	0.3305(2) 0.0221(2) 0.0048(4) 0.004(1)	0.004(2)	0.0195(5)	0.0056(7)	0.531(6)	0.001(2)	0.6558(6)
LT′-$Ni_{1.38}Sn$	673	0.0137(5) 0.0142(4)	0.0421(4) 0.0119(7) 0.034(1)	0.3315(2) 0.0189(2) 0.0038(4) 0.003(2)	0.003(2)	0.0174(5)	0.0052(7)	0.454(6)	0.009(2)	0.6602(7)
LT′-$Ni_{1.38}Sn$	473	0.0121(5) 0.0140(4)	0.0471(4) 0.0164(7) 0.028(1)	0.3307(2) 0.0213(2) 0.0045(4) 0.001(1)	0.006(2)	0.0186(5)	0.0046(7)	0.518(6)	0.001(2)	0.6587(7)
LT′-$Ni_{1.35}Sn$	673	0.0160(5) 0.0152(4)	0.0372(4) 0.0129(8) 0.029(2)	0.3324(2) 0.0169(2) 0.0050(4) 0.007(1)	0.008(2)	0.0151(6)	0.0067(8)	0.382(7)	0.007(3)	0.6635(9)
LT′-$Ni_{1.35}Sn$	473	0.0138(5) 0.0132(4)	0.0452(4) 0.0150(7) 0.024(2)	0.3310(2) 0.0204(2) 0.0060(4) 0.003(1)	0.007(2)	0.0184(5)	0.0065(7)	0.499(6)	0.000(2)	0.6603(7)

[a] Final annealing temperature before quenching.
[b] Not relevant for the commensurate LT case (cf. Table 1).

Table 4
'Conventional' structure parameters for LT-$Ni_{1+\delta}Sn$ for $t=1/8$ (cf. Table 1): *Pbnm*, $a_{LT}=2a_{orth}$, $b_{LT}=3^{1/2}b_{orth}$, $c_{LT}=c_{orth}$

Atom	T_{ann} (K)[a]	x[b,c]	y[b]	z[b]	occupancy occ^M
LT-$Ni_{1+\delta}Sn$, relation of fractional coordinates with parameters of average structure and the modulation waves (cf. Table 1)					
Ni(1)	—	$1/8+u^{Ni(1)}_{x,s,2}/2$	$1/4+u^{Ni(1)}_{y,s,1}/2^{1/2}$	$0+u^{Ni(1)}_{z,s,1}/2^{1/2}$	1
Ni(2a)[d]	—	$1/8+(u^{Ni(2)}_{x,c,1}/2^{1/2}+u^{Ni(2)}_{x,s,2})/2$	$1/4+y^{Ni(2)}_{av}+u^{Ni(2)}_{y,s,1}/2^{1/2}$	1/4	$\delta+p^{Ni(2)}_{s,1}/2^{1/2}$
Ni(2b)[d]	—	$1/8+(-u^{Ni(2)}_{x,c,1}/2^{1/2}+u^{Ni(2)}_{x,s,2})/2$	$5/4-y^{Ni(2)}_{av}+u^{Ni(2)}_{y,s,1}/2^{1/2}$	3/4	$\delta-p^{Ni(2)}_{s,1}/2^{1/2}$
Sn(a)	—	$1/8+(-u^{Sn}_{x,c,1}/2^{1/2}+u^{Sn}_{x,s,2})/2$	$5/4-y^{Sn}_{av}+u^{Sn}_{y,s,1}/2^{1/2}$	3/4	1
Sn(b)	—	$1/8+(u^{Sn}_{x,c,1}/2^{1/2}+u^{Sn}_{x,s,2})/2$	$1/4+y^{Sn}_{av}+u^{Sn}_{y,s,1}/2^{1/2}$	1/4	1
LT-$Ni_{1.50}Sn$, as calculated from results listed in Table 3					
Ni(1)	673	0.1251(4)	0.2352(3)	0.0035(4)	1
	473	0.1251(4)	0.2341(3)	0.0046(4)	
Ni(2a)	673	0.1264(4)	0.9089(4)	1/4	0.990(4)
	473	0.1271(4)	0.9089(4)	1/4	1.006(4)
Ni(2b)	673	0.1236(4)	0.5911(4)	3/4	0.010(4)
	473	0.1229(4)	0.5911(4)	3/4	−0.006(4)
Sn(a)	673	0.1413(2)	0.9019(2)	3/4	1
	473	0.1419(2)	0.9017(2)	3/4	
Sn(b)	673	0.0961(2)	0.5603(2)	1/4	1
	473	0.0952(2)	0.5595(2)	1/4	
LT-$Ni_{1.47}Sn$, as calculated from results listed in Table 3					
Ni(1)	673	0.1261(4)	0.2352(3)	0.0047(5)	1
	473	0.1255(4)	0.2353(3)	0.0042(4)	
Ni(2a)	673	0.1261(4)	0.9091(5)	1/4	0.946(4)
	473	0.1285(4)	0.9096(5)	1/4	0.940(4)
Ni(2b)	673	0.1239(4)	0.5909(5)	3/4	−0.008(4)
	473	0.1215(4)	0.5904(5)	3/4	−0.002(4)
Sn(a)	673	0.1406(2)	0.9025(2)	3/4	1
	473	0.1405(1)	0.9025(2)	3/4	
Sn(b)	673	0.0975(2)	0.5615(2)	1/4	1
	473	0.0966(1)	0.5611(2)	1/4	

[a] Final annealing temperature before quenching.
[b] Taking into account the shift in origin indicated in Fig. 2. For an undistorted structure (with respect to displacements) all u values would be 0, $y^{Ni(2)}_{av}=2/3$ and $y^{Sn}_{av}=1/3$. Standard deviations do not take into account correlations between $u^{Sn}_{x,c,1}$ and $u^{Sn}_{x,s,2}$, as well as between y^{Sn}_{av} and $u^{Sn}_{y,c,1}$, respectively.
[c] The displacements along $[100]_{orth}$ in terms of fractional coordinates have to be divided by two, because the a-axis is doubled by going from the average unit cell (for which the shifts were calculated) to the LT unit cell with *Pbnm* symmetry.
[d] $u^{Ni(2)}_{x,s,2}$ and $u^{Ni(2)}_{y,s,1}$ could not be refined and were set to 0 (see Section 3).

determined from X-ray powder patterns calibrated by Ge powder standard are listed in Table 2.

Rietveld refinements of powder diffraction data on LT-$Ni_{1+\delta}Sn$ with $\delta=0.47$ and 0.50 quenched from 473 to 673 K (Fig. 3a), respectively, give convincing results only for the sections at $t=1/8+n/4$ ($n\in\mathbb{Z}$) which correspond to the *Pbnm* three-dimensional space group symmetry of the known LT structure (Tables 2 and 3). From the parameters of the modulation functions, the corresponding 'conventional' fractional coordinates and occupancies were calculated (cf. Table 4).

Only two positional parameters could be refined for Ni(2), $u^{Ni(2)}_{x,c,1}$ and $y^{Ni(2)}_{av}$. $u^{Ni(2)}_{x,s,2}$ and $u^{Ni(2)}_{y,s,1}$ diverge when not set fixed to zero. This can be easily understood, when the corresponding fractional coordinates are considered (Table 4): The occupational modulation for Ni(2) leads to virtually complete order with occupancies close to 1 for Ni(2a) and 0 for Ni(2b). Thereby, only the x and y fractional coordinates of the Ni(2a) site can be refined but not those of Ni(2b). Therefore, the parameters $u^{Ni(2)}_{x,s,2}$ and $u^{Ni(2)}_{y,s,1}$, which would contain the difference between the displacements of the two different Ni(2) sites, cannot be determined. This means that although fractional coordinates can be calculated for the 'virtual' Ni(2b) site from $u^{Ni(2)}_{x,c,1}$ and $y^{Ni(2)}_{av}$, this result has only a formal meaning, because it was fitted only on the basis of the electron density due to Ni(2a). The Sn atoms have the same type of positional modulation parameters as Ni(2), but they can all be refined, because both Sn(a) and Sn(b) are fully occupied.

Trial refinements for the second high-symmetric sections with $t=0+n/4$ ($n\in\mathbb{Z}$) of *Pmnm* symmetry did not give convincing results. Although convergence of the Rietveld refinements could be achieved, the R_{Bragg}

Table 5
Interatomic distances (Å) for HT-$Ni_{1.50}Sn$ quenched from 1023 K (calculated purely from the cell parameters) and for LT-$Ni_{1.50}Sn$ quenched from 473 K[a]

Sample	Environment of Ni(1)	Environment of Ni(2)	Environment of Sn	
HT-$Ni_{1.50}Sn$[b]	6 × Sn: 2.701	3 × Sn: 2.370	3 × Ni(2): 2.370	
	2 × Ni(1): 2.590	2 × Sn: 2.590	2 × Ni(2): 2.590	
	6 × 0.5 Ni(2): 2.701	6 × Ni(1): 2.701	6 × Ni(1): 2.701	
LT-$Ni_{1.50}Sn$	1 × Sn(a): 2.604(3)	1 × Sn(b): 2.503(3)	Sn(a)—	Sn(b)—
	1 × Sn(b): 2.658(2)	1 × Sn(b): 2.504(3)	1 × Ni(2a): 2.574(3)	1 × Ni(2a): 2.503(3)
	1 × Sn(b): 2.671(3)	1 × Sn(a): 2.574(3)	2 × Ni(2a): 2.601[c]	1 × Ni(2a): 2.504(3)
	1 × Sn(a): 2.701(3)	2 × Sn(a): 2.601[c]	2 × Ni(1): 2.604(3)	2 × Ni(1): 2.658(2)
	1 × Sn(a): 2.716(2)	2 × Ni(1): 2.644(3)	2 × Ni(1): 2.701(3)	2 × Ni(1): 2.671(3)
	1 × Sn(b): 2.892(3)	2 × Ni(1): 2.648(3)	2 × Ni(1): 2.716(2)	2 × Ni(1): 2.892(3)
	1 × Ni(1): 2.550(2)	2 × Ni(1): 2.693(4)		
	1 × Ni(1): 2.646(2)			
	1 × Ni(2a): 2.644(3)			
	1 × Ni(2a): 2.648(3)			
	1 × Ni(2a): 2.693(4)			

[a] For the LT-phase distances involving the virtually unoccupied Ni(2b) are not listed.
[b] The standard deviations of the interatomic distances for the HT phase were omitted. Because of the—due to symmetry—fixed fractional coordinates they would only be determined by the standard deviation of the unit cell parameters.
[c] The standard deviations of these axial distances Ni(2a)···Sn are mainly determined by those of the unit cell parameters.

parameters are larger by a factor of roughly two than those for the *Pbnm* section. For the *Pmnm* case, the occupational modulation would generate three unequivalent Ni(2) sites. One of these is located on the nodes of the occupation modulation function giving occupancies of $p^{Ni(2)} = \delta$ and the other two would be filled up and depleted, respectively, to a degree far out of the sensible range of occupation $0 \leqslant occ^{Ni(2)} \leqslant 1$. Therefore, the *Pmnm* case has no physical relevance. Refinements using the general symmetry $P2_1nm$, do not give results superior to *Pbnm*.

For the Rietveld refinements of the LT′ phase (Fig. 3b, and Tables 2 and 3) $u^{Sn}_{y,c,2}$, $u^{Sn}_{x,c,3}$ and $u^{Sn}_{y,s,3}$ were used additional to the modulation parameters refined for the LT phase. Especially $u^{Sn}_{x,c,3}$ has a significant impact on the residuals (improvement of the R_{Bragg} values for the first-order satellites by 10–30%). Compared to LT, no additional parameters for Ni(1) and Ni(2) were refined, because they gave no additional improvement of the results. Due to the large amplitude of the occupational modulation as given by $p^{Ni(2)}$, there are ranges of x_4 in which the occupancy, $occ^{Ni(2)} = \delta + p^{Ni(2)}_{s,1} \sin 2\pi x_4$, is considerably out of the physical relevant range $0 \leqslant occ^{Ni(2)} \leqslant 1$. A refinement of a second harmonic term for the occupation modulation, $p^{Ni(2)}_{c,2}$, gave slightly negative values for this parameter, which decreases the x_4 ranges with $occ^{Ni(2)} < 0$ or $occ^{Ni(2)} > 1$. However, these ranges remain considerable, and since the refinement of $p^{Ni(2)}_{c,2}$ does not significantly improve the residuals, $p^{Ni(2)}_{c,2}$ was not considered in the final refinements.

Trial refinements using a *Crenel*-type description of occupational modulation gave considerably worse residuals than those using the first-order harmonic description of occupational modulation: The R_{Bragg} values for first-order satellites increase by 20–50%. The origin of the problems concerning the occupancies of Ni(2) are discussed in Section 4.2.

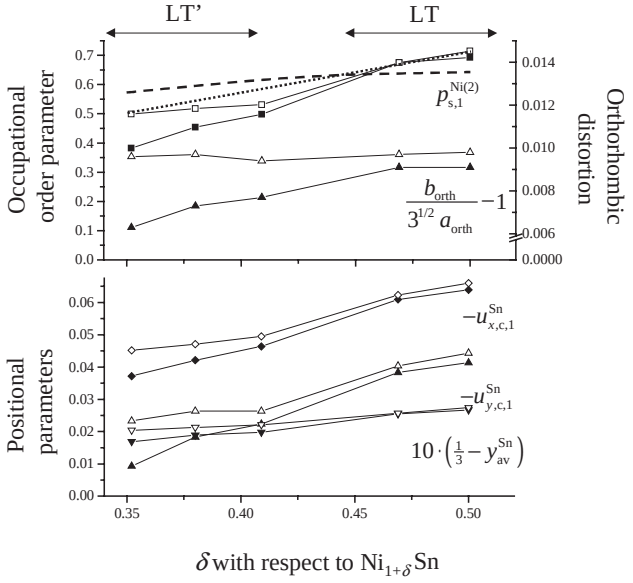

Fig. 4. Occupational modulation parameter, orthorhombic distortion (top), and selected displacive modulation parameters for Sn (bottom), compare Tables 2 and 3. The ranges for the LT and LT′ phases are indicated. Filled/open symbols represent data quenched from 673 K/473 K. In the top part, the dotted line represents the theoretical maximum value for $p^{Ni(2)}_{s,1}$ corresponding to the fully ordered LT structure with $p^{Ni(2)}_{s,1,max} = 2^{1/2}\delta$. The dashed curve represents $p^{Ni(2)}_{s,1,max} = (2/\pi)\sin \pi\delta$, the expected limiting value for a fully ordered LT′ structure with *Crenel-type* occupational modulation of Ni(2).

4. Discussion

4.1. Interpretation of the structural data of the LT phase

The crystal structures of the LT phase (Ni_3Sn_2) have been discussed previously mainly by *describing* the ordering pattern of Ni(2) and the atomic displacements without further *interpretation* [4,6]. Considerations which compare chemical bonding in the LT- and HT phases on the basis of the bond lengths [19] must be regarded as meaningless due to the wrong interpretation of apparent unusual short distances Ni···Sn in the HT phase (see below). Therefore, an interpretation of the structural parameters found for LT-$Ni_{1.47}Sn$ and LT-$Ni_{1.50}Sn$ quenched from 673 to 473 K, respectively, will be given here. The main emphasis will be put on the differences between the HT and LT phase structures. If specific cell parameter data or interatomic distances are used in the course of the following considerations, they refer to the data of HT-/LT-$Ni_{1.50}Sn$ quenched from 1023 K/473 K (see Table 5).

The phase transition LT→HT is a typical order–disorder transition. The degree of occupational ordering is given by the 'primary' order parameter $p_{s,1}^{Ni(2)}$, which basically quantifies the amount of transfer of Ni(2) from the 'wrong' (Ni(2b)) to the 'right' (Ni(2a)) site (Table 4). For $\delta \leqslant 0.50$ the maximum possible value results from $occ^{Ni(2b)} = 0$ which gives $p_{s,1,max}^{Ni(2)} = 2^{1/2}\delta$ (see Table 4). For both $Ni_{1.47}Sn$ and $Ni_{1.50}Sn$, respectively, the ordering can be regarded as virtually complete, or in some cases even slightly too high (see Fig. 4), which is, however, not regarded as significant.

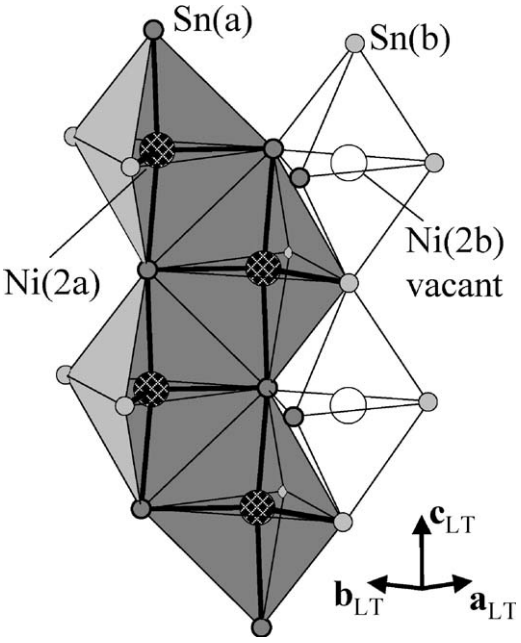

Fig. 5. Occupied and unoccupied Sn_5 trigonal-bipyramids in LT-$Ni_{1.50}Sn$ showing the expansion of the basal Sn_3 triangles of the occupied trigonal-bipyramids.

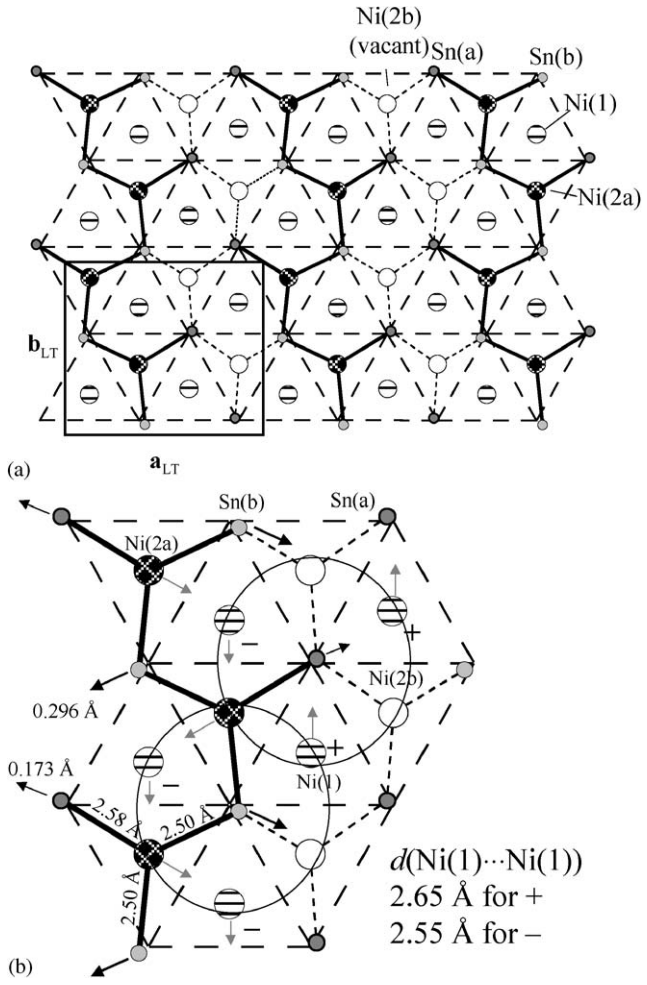

Fig. 6. LT-$Ni_{1.50}Sn$ (view along [001]): (a) Sn (Sn(a) and Sn(b)) and Ni(2) (fully occupied Ni(2a) and 'virtual', vacant Ni(2b) sites at $z = 1/4$ as well as Ni(1) sites at $z \approx 0$ and ≈ 0.5. The dashed lines interconnect the 'ideal' Sn sites, illustrating the direction of the displacements of Sn. (b) Enlarged part of (a). The arrows indicate the directions of the displacements within the shown plane. For Ni(1)+ or − signs indicate, whether Ni(1) atoms are located at $0 - u_{z,s,1}^{Ni(1)}$ and $0.5 + u_{z,s,1}^{Ni(1)}$ or at $0 + u_{z,s,1}^{Ni(1)}$ and $0.5 - u_{z,s,1}^{Ni(1)}$, respectively, i.e., whether the Ni(1) atoms below and above $z = 1/4$ are shifted away from or towards each other. The circles indicate the environments of Sn(a) and Sn(b) as shown in Fig. 7.

The occupational ordering scheme for Ni(2) by itself reduces the symmetry from $P6_3/mmc$ (HT phase) to $Pbnm$ (LT phase). This can be done via a formal sequence of space groups as follows $P6_3/mmc$ (a_{HT},a_{HT},c_{HT}) — $t3 \rightarrow Cmcm$ $(a_{HT},3^{1/2}a_{HT},c_{HT})$ — $k2 \rightarrow Pbcm$ $(a_{HT},3^{1/2}a_{HT},c_{HT})$ — $k2 \rightarrow Pbnm$ $(2a_{HT},3^{1/2}a_{HT},c_{HT})$ [20]. Additional (secondary) structural changes occur, but they do not lower the symmetry further than the occupational order does. These additional changes which can be regarded as induced by the occupational ordering are:

- considerable displacements of the atoms from their ideal positions (cf. Tables 3 and 4)

- an orthorhombic distortion of the unit cell given by $b_{orth}/(3^{1/2}a_{orth}) - 1$, which is 0 for the undistorted HT case and >0 for all LT/LT′ cases.
- an increase of the (effective) *c*/*a* ratio $c_{orth}/(a_{orth} \times b_{orth}/3^{1/2})^{1/2}$ [2]
- a decrease of the unit cell volume.

The occurrence of the secondary changes can be explained—on the basis of the occupational ordering scheme—by the spatial requirements of the Ni(2) atoms in their environments. One may first—very much simplified—compare the distances listed in Table 5 with the sums of the metallic radii for a coordination of 12 of Ni (1.246 Å) and Sn (1.623 Å) [21]: Hence, distances of 2.49 Å for Ni···Ni, 2.87 Å for Ni···Sn, and 3.24 Å for Sn···Sn would be expected. Only the observed Ni···Sn distances are considerably smaller than the 'expected' ones. Therefore, the Ni···Sn contacts will be considered further on as the main basis for the discussion. The shortest reliable (according to own knowledge) Ni···Sn distance reported in literature for a well-ordered structure is 2.43 Å in $LuNiSn_2$ [22].

For the HT phase, in which all atoms are located on sites without free positional parameters the (apparent) interatomic distances can be calculated just from the unit cell parameters (Table 5). The thus obtained distances Ni(2)···Sn of 2.37 Å within the $a-b$-plane are extremely short, even compared to the value of $LuNiSn_2$ (see above). Indeed, there are indications, that on a local scale, considerable static displacements of the Sn atoms occur within the $z = 1/4$ plane as followed by the shape of diffuse scattering in electron diffraction patterns [23] as well as investigation of the electron densities around the Sn position [24]. Therefore, the real Ni(2)···Sn distances are longer than 2.37 Å. The static displacements in the HT phase have their counterpart in the LT phase: the Ni(2) atoms, which are 'too large' for the undistorted trigonal-bipyramidal environment, lead to an expansion of their surrounding trigonal-bipyramids within the a-b-plane whereas those unoccupied by Ni(2) (Ni(2b) sites) are contracted (Figs. 5 and 6). The shortest Ni(2a)···Sn distance is now 2.50 Å (Table 5). Since all Sn atoms are exactly located at $z = 1/4$ (and 3/4) (these planes are mirror planes *m*), their displacements can be visualized by just considering such a plane (see Fig. 6).

The ordering pattern of Ni(2) leads to two crystallographically unequivalent Sn atoms (Sn(a) and Sn(b)) which are displaced into different *directions*. The Sn(a) atoms are displaced from their ideal positions ($y_{av} = 1/3$, $u^{Sn}_{x,c,1} = u^{Sn}_{x,s,2} = u^{Sn}_{y,s,1} = 0$) by 0.17 Å into the direction of a pair of Ni(1) atoms at $z = 0$ and $z = 1/2$.

[2] The dimensionless variables axial ratio and orthorhombic distortion do not contain the overall increase of the lattice parameters with increasing δ and are, therefore, advantageous for discussing the variation of structural parameters with changing δ.

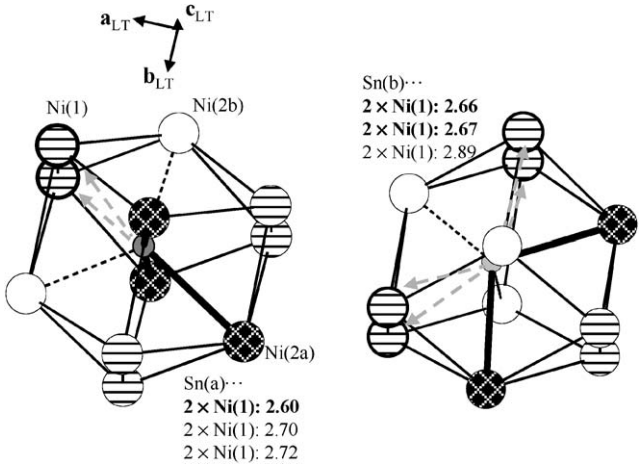

Fig. 7. Local environment of Sn(a) and Sn(b) by a trigonal-bipyramid of Ni(2a)/Ni(2b) sites and a trigonal-prism of Ni(1) atoms. The particular Ni(1) atoms governing the magnitude of the displacements of Sn(a) and Sn(b), respectively, are highlighted by thick edges. The corresponding Sn···Ni(1) distances (also indicated by arrows) are given in bold letters.

This direction can be understood by a simple radial displacement of Sn(a) by the single (within the $z = 1/4$ plane) nearest-neighbour Ni(2a) atom (two further Ni(2a) atoms are also close at $z = -1/4$ and $z = 3/4$, below and above Sn(a) at $z = 1/4$). A larger displacement of 0.30 Å is observed for Sn(b), which is directed towards an empty Ni(2b) site. The direction of this displacement (but not its magnitude) can be explained by vector addition of two radial displacements by two close Ni(2a) neighbours within the same $z = 1/4$ plane (Sn(b) has no nearest Ni(2a) neighbours below and above that plane).

The different *magnitudes* of the displacements of Sn(a) and Sn(b) can be explained by the different easiness of displacement of Sn into the corresponding directions. This easiness is determined by the repulsion of the displaced Sn by those Ni(1) atoms which are located in the displacement direction. In the HT phase, the apparent distance Sn···Ni(1) is 2.701 Å, which is compared to Sn···Ni(2) not very short. These distances are shortened if the Sn atoms are displaced out of the centre of the approximate trigonal-prism formed by the six surrounding Ni(1). Sn(b) is displaced towards a sideways rectangle of the Ni(1) prism, i.e., towards an empty Ni(2b) site (Figs. 6 and 7). By that, the four distances Sn(b)···Ni(1) are shortened down to 2.66–2.67 Å, whereas the distances to the opposite pair of Ni(1) atoms are elongated (Fig. 7). On the contrary, Sn(a) is displaced directly towards a sideways edge of the prism formed by two Ni(1) atoms. In this less easy displacement direction, the Sn atoms approach the Ni(1) atoms much faster than for the displacement direction of Sn(b). Therefore, although Sn(a) is displaced by a

Table 6
Positional modulation parameters from structure determinations of $Ni_{1.50}Sn$ as well as of isotypic $Co_{1.42}Sn$ and $Mn_{1.50}Sn$

	$Ni_{1.50}Sn$[a]	$Ni_{1.486}Sn$[b,c,d] [4]	$Mn_{1.50}Sn$[c,d] [27]	$Co_{1.42}Sn$[b,c,d] [4]
$u^{Sn}_{x,c,1}$	−0.0660(3)	−0.075(4)	−0.072(4)	−0.069(4)
$u^{Sn}_{x,s,2}$	−0.0129(3)	−0.015(3)	−0.021(3)	0.007(3)
y^{Sn}_{av}	0.3289(1)	0.334(2)	0.328(1)	0.330(2)
$u^{Sn}_{y,s,1}$	−0.0274(2)	−0.026(3)	−0.028(2)	−0.028(4)
$u^{Ni(1)}_{x,s,2}$	0.0002(8)	−0.015(2)	−0.004(4)	−0.010(6)
$u^{Ni(1)}_{y,s,1}$	−0.0225(4)	−0.0208(8)	−0.028(3)	−0.027(3)
$u^{Ni(1)}_{z,s,1}$	0.0065(6)	0.006(1)	0.007(3)	0.025(4)
$u^{Ni(2)}_{x,c,1}$	0.006(1)	0.010(3)	0.011(4)	0.03(1)
$y^{Ni(2)}_{av}$	0.6589(4)	0.658(1)	0.649(2)	0.678(4)
orth. distortion $(b_{orth}/3^{1/2}a_{orth}) - 1$	0.0098	0.0093	0.0167	0.0015[e]

[a] X-ray powder diffraction, this work; sample quenched from 473 K.
[b] Composition determined by refinement of $occ^{Ni(2a)/Co(2a)}$; $occ^{Ni(2b)/Co(2b)} = 0$.
[c] Calculated from 'conventional' fractional coordinates listed in literature.
[d] Rietveld refinement on the basis of neutron powder diffraction.
[e] Calculated from cell parameters from Rietveld analysis of neutron diffraction data. According to better-resolved X-ray powder diffraction patterns, no orthorhombic distortion is visible.

smaller magnitude than Sn(b), two Ni(1)⋯Sn(a) distances of only 2.60 Å result.

The direction of the displacements of Ni(1) can be explained by the tendency to 'evade' the shortened distances Ni(1)⋯Sn as a result of the just discussed displacements of Sn. The distances mentioned above already consider these displacements of Ni(1). If Ni(1) is, however, artificially put on its ideal position ($u^{Ni(1)}_{x,s,2} = u^{Ni(1)}_{y,s,1} = u^{Ni(1)}_{z,s,1} = 0$), and distance to the six nearest Sn neighbours is calculated, one finds Sn⋯Ni(1) distances in the range of 2.54–2.95 Å. With the observed displacements, the distances range only within 2.60–2.89 Å (see Table 5), and are, therefore, more uniform. In particular, the occurrence of a smaller shortest Sn(a,b)⋯Ni(1) distance is prevented.

The displacements of Ni(2a) are the least pronounced ones, and can also be understood as an accommodation to the other displacements. If Ni(1) and Sn(*a*,*b*) have the experimentally observable coordinates and Ni(2a) is put on its ideal sites without displacements ($y_{av} = 2/3$, $u^{Ni(2)}_{x,c,1} = 0$), especially the Ni(2a)⋯Ni(1) distances would vary strongly, i.e., within 2.60–2.73 Å, whereas with the observed displacements more uniform distances in a range of 2.65–2.69 Å would result (Table 5).

Upon going from the HT to the LT phase, there are not only long-range occupational and positional modulations, but also a distortion of the lattice (relative to a_{HT}, $3^{1/2}b_{HT}$ and c_{HT}) occurs: Strains of -7.6×10^{-3} for a_{orth}, 1.9×10^{-3} for b_{orth} and 3.1×10^{-3} for c_{orth} are found, leading also to a small decrease in unit cell volume. The contraction in the $[100]_{orth}$ direction can be understood by taking into account the zig-zag chains of occupied and unoccupied trigonal-bipyramids Sn_5 along $[010]_{orth}$: The empty chains allow the occupied ones to become closer along $[100]_{orth}$, and the aggregation of Ni(2) in the occupied zig-zag chains causes the elongation along $[010]_{orth}$. This leads to the observed orthorhombic distortion.

The elongation along $[001]_{orth}$ may be understood by an expansion of the trigonal-bipyramids not only in basal, but also in apical direction (but to a lesser extent) which leads to a change in the effective *c*/*a* ratio: There are infinite chains ⋯Ni(2a)–Sn(a)–Ni(2a)–Sn(a)⋯ along $[001]_{orth}$ (cf. Fig. 5) and the Sn(a) and Ni(2a) atoms are located on mirror planes …*m* in *Pbnm*. Consequently, there cannot be displacement modulations along $[001]_{orth}$, but, instead, the displacements cumulate and lead to the observed elongation of c_{LT} compared to c_{HT}. In the HT phase probably local static displacements of Sn $[001]_{HT}$ direction exist. Such displacements in fact exist in ordered modifications of Cu_6Sn_5 ($Cu(1)Cu(2)_{1/5}Sn$, [25,26]), in which 'isolated' $Cu(2)Sn_5$ trigonal-bipyramids occur.

All prominent modulation parameters are smaller for LT-$Ni_{1.47}Sn$ than for LT-$Ni_{1.50}Sn$ (Fig. 4). For the occupational modulation parameter $p^{Ni(2)}_{s,1}$ this is explained by its theoretical maximum value of $p^{Ni(2)}_{s,1} = 2^{1/2}\delta$ (given by $0 \leqslant occ^{Ni(2)} \leqslant 1$). Likewise, the secondary changes relative to the HT phase, like the atomic displacements and the orthorhombic distortions are reduced (Fig. 4). This can be explained by the generation of vacancies on the Ni(2a) sites by going from $Ni_{1.50}Sn$ to $Ni_{1.47}Sn$. Therefore, the discussed mechanisms of displacement cannot work to a full extent and reduce the 'secondary' order parameters.

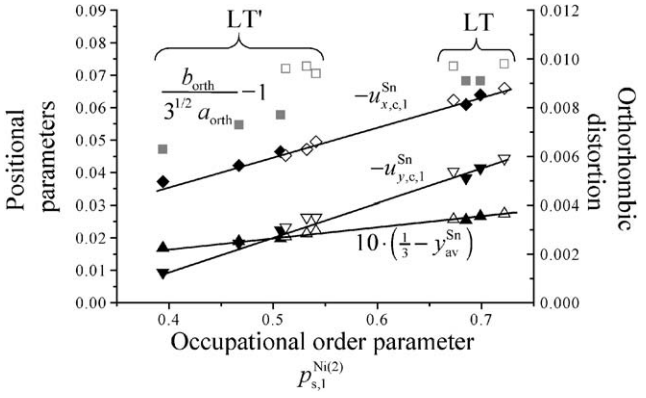

Fig. 8. Plot of the orthorhombic distortion (grey) and selected displacive modulation parameters (black) as a function of the occupational modulation parameter. Filled/open symbols correspond to data from samples quenched from 673 K/473 K. The lines for the modulation parameters serve as a guide for the eye.

For both compositions, a comparison between the modulation parameters for the samples quenched from 673 to 473 K indicates somewhat more exhibited ordering for the lower annealing temperature. This becomes even more evident for the 'secondary' order parameters like orthorhombic distortion and displacement parameters of Sn than for the occupational order parameters. The observed dependence of the order parameters from the annealing temperature would be expected from some pretransitional disorder below the actual phase transition temperature.

The structural parameters obtained here for LT-$Ni_{1.50}Sn$ agree well with those from previous neutron powder diffraction data [4], except for a significantly negative $u^{Ni(1)}_{x,s,2}=-0.015$, which was not obtained from the present data (cf. Table 6). The only intermetallic phases isotypic with LT-$Ni_{1.50}Sn$ for which refined structural parameters exist are $Mn_{1.50}Sn$ (Mn_3Sn_2) [27] and $Co_{1.42}Sn$ (Co_3Sn_2) [4].

The positional modulation parameters of the manganese compound are somewhat larger than for LT-$Ni_{1.50}Sn$, and the orthorhombic distortion is considerably larger. These differences between the manganese and the nickel compounds may be understood by taking into account the larger metallic radius of Mn compared to that of Ni (1.264 Å instead of 1.246 Å [21]). Therefore, the displacements of the atoms and the unit cell distortion occurring upon occupational ordering of Mn on trigonal-bipyramidal sites are expected to be even larger than in $Ni_{1.50}Sn$, in agreement with the observations.

The intermediate character of the metallic radius of Co (1.252 Å [21]) suggests that the structural characteristics of $Co_{1.42}Sn$ (Co_3Sn_2) should be intermediate between $Ni_{1.50}Sn$ and $Mn_{1.50}Sn$. The results of a Rietveld refinement on the basis of neutron diffraction data of $Co_{1.42}Sn$ (composition from Rietveld refinement, nominal composition was $Co_{1.45}Sn$ [4]) show roughly the same tendencies as for $Ni_{1.50}Sn$ and $Mn_{1.50}Sn$, but structural parameters of the cobalt compound seem to be too inaccurate for a comparison with those of the other compounds (e.g., an unreasonably short distance of Co⋯Sn of 2.33(4) Å would result from the data listed in Table 6). Surprisingly, there is no orthorhombic lattice distortion observed for the Co compound [4,28].

4.2. Structural parameters of incommensurate LT′ in comparison to the commensurate LT phase

In contrast to results for the LT phase, the degree of occupational and secondary ordering in the examined LT′ phase samples varies strongly with the final annealing temperature (Fig. 4). The differences between the states quenched from 673 to 473 K state can—at least partially—be ascribed to a decrease of the phase transition temperatures LT′-HT upon going from ~$Ni_{1.50}Sn$ to lower Ni contents (A. Leineweber, unpublished and [4]) and a higher degree of pretransitional disordering.

The evolution of the modulation parameters for the LT and LT′ phases as a function of δ (Fig. 4) suggests that in spite of the change of the modulation vector from $\mathbf{q}=\mathbf{a}^*_{orth}/2$ to $\mathbf{q}=\alpha\mathbf{a}^*_{orth}$ with $\alpha<1/2$ there are strong analogies between the structures of the two phases, which go far beyond the common superspace group symmetry $Cmcm(\alpha00)0s0$. A way slightly different from Fig. 4 to reveal the parallels between the LT and the LT′ phases is employed in Fig. 8 by plotting various secondary order parameters vs. the primary order parameter $p^{Ni(2)}_{s,1}$: the displacive modulation parameters increase approximately linearly with $p^{Ni(2)}_{s,1}$—irrespective of δ and quenching temperature. This shows that in the LT′ phase the occupational modulation has quite similar consequences as for the LT phase (cf. Section 4.1), in particular, concerning the displacements of Sn due to the spatial needs of Ni(2). However, the orthorhombic distortion does not depend in a simple way on $p^{Ni(2)}_{s,1}$, e.g., the 473 K data apparently do not vary with $p^{Ni(2)}_{s,1}$, and the 673 K data show a different behaviour than the 473 K data. Probably, there is a superposition of the effect of order and the effect of overall composition, which makes the orthorhombic distortion more difficult upon going from lower to higher nickel contents. This is also confirmed for the absence of an orthorhombic lattice distortion in an orthorhombic LT″ phase with $\delta>0.5$ (A. Leineweber, unpublished).

For all six sets of structural data of LT′-phase samples (Table 3), the values of the occupational modulation parameter $p^{Ni(2)}_{s,1}$ are so high that the occupancy of Ni(2) assumes values significantly out of the physically sensible range of $0\leqslant occ^{Ni(2)}\leqslant 1$ for certain ranges of

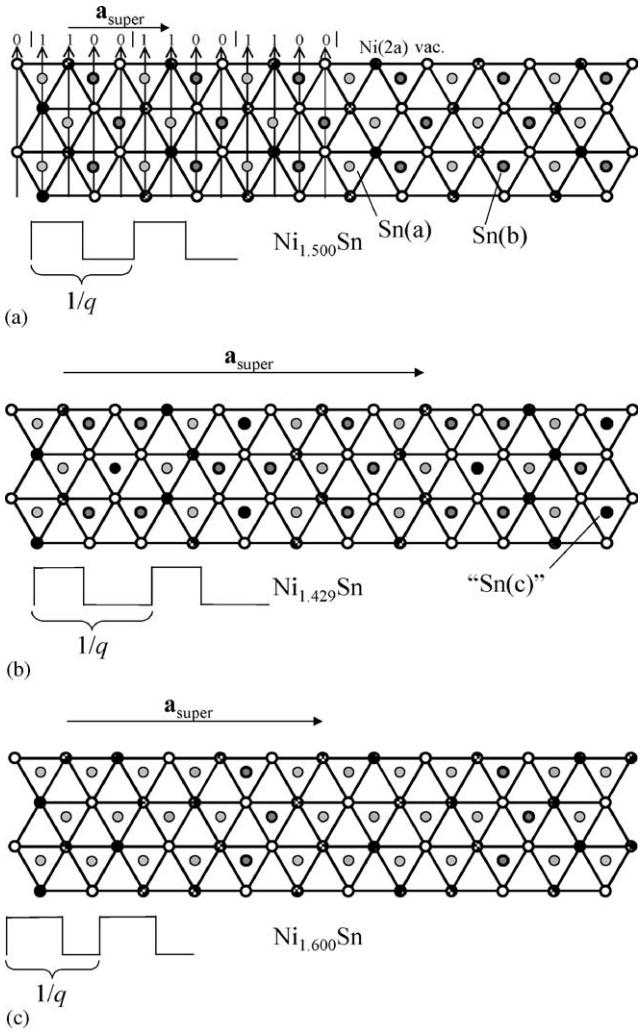

Fig. 9. Model structures for $Ni_{1+\delta}Sn$ indicating the distribution of 'Ni(2a)' and vacancies (vac) on the trigonal-bipyramidal interstices. A plane at $z = 1/4$ is shown for (a) $Ni_{1.50}Sn$, (b) $Ni_{1.429}Sn$, and (c) $Ni_{1.600}Sn$. In (a) the arrows perpendicular to the superstructure cell vector $\mathbf{a}_{super}$ indicate how the '1's and '0's are related with the ordering pattern. Furthermore, Sn(*a*,*b*,*c*) indicate Sn atoms at $z = 1/4$ with 1, 2, and 0 nickel neighbours within the shown plane. The *Crenel*-type modulation wave with the wavelength $1/q$ is indicated below the structures.

x_4. This problem is frequently encountered for strong occupational modulations if they were described by a Fourier series of a limited number of terms [14]. The failure to overcome this situation in the present cases by employing a *Crenel*-type function indicates that the ordering of Ni(2) is incomplete: All values refined for the occupational modulation parameter $p_{s,1}^{Ni(2)}$ are considerably smaller than those values which would be expected for a *Crenel*-type occupational ordering, $p_{s,1,max}^{Ni(2)} = (2/\pi)\sin\pi\delta$ (cf. Eq. (1) and Fig. 4). Since the present diffraction data did not allow to determine more than only the first Fourier coefficient of the 'real' non-*Crenel*-type occupational modulation function, the situation

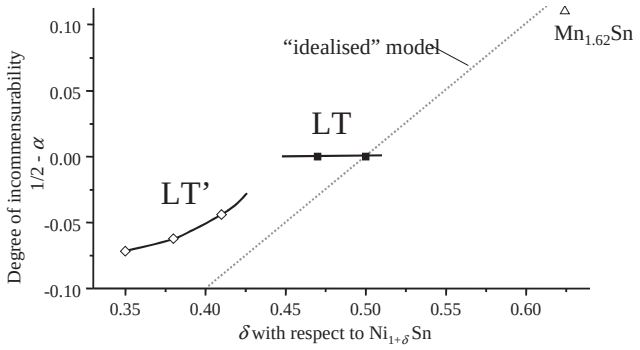

Fig. 10. 'Degree' of incommensurabilty $1/2 - \alpha$ with $\mathbf{q} = \alpha \cdot \mathbf{a}^*_{orth}$ (bottom) as a function of composition for LT′-, LT-$Ni_{1+\delta}Sn$ (this work) and $Mn_{1.62}Sn$ [13]. The experimental points are connected to guide the eye. The evolution of α with varying δ for the idealized structure model (Fig. 9) is indicated by a dotted line.

with x_4 ranges with Ni(2) occupancies outside $0 \leqslant occ^{Ni(2)} \leqslant 1$ was accepted as the best available approximation. The assumption of an *incomplete* Ni(2) ordering in all LT′-phase samples is also backed by the varying degree of ordering in the samples quenched from 673 K and from 473 K (see above).

4.3. Derivation of a simplified structure model for the LT′ phase

An idealized model for ordered $Ni_{1+\delta}Sn$ can be constructed by adopting *Crenel*-type occupation modulations for Ni(2). This model will allow at least a qualitative understanding for the experimentally observed evolution of α as a function of the composition expressed as δ in the LT and LT′ phases.

Imagine at first a single plane at $z = 1/4$ with the Ni(2) distributed as in the Ni_3Sn_2 ideal structure (Fig. 9a). The Ni(2) distribution in that plane can be described by the projection of the occupancies of rows along $\mathbf{b}_{orth}$ onto $\mathbf{a}_{orth}$ giving a sequence of '1's and '0's. For ideal $Ni_{1.50}Sn$, one finds the sequence |1100|1100|1100|1100| (Fig. 9a), where the '11' pairs correspond to the *zig-zag* chains of Ni(2) (cf. Section 4.1), and where the '|' highlights the periodicity of the sequence along $[100]_{orth}$. The modulation function has a wavelength of $\lambda = 2a_{orth}$. Therefore, $|\mathbf{q}| = q = 1/\lambda = 1/2\mathbf{a}^*_{orth} (\alpha = 1/2)$ follows.

Obviously, new superstructures of changed Ni(2) content δ can be generated by removing or introducing either '1' rows or '0' rows from or into the layer in a periodic manner. Assume now, that one adds a certain amount of '0' rows to the '00' pairs, e.g., by introducing two '0' rows into two of three initial |1100| cells. By this one gets the sequence ||11000|11000|1100|| (inserted rows indicated in bold; double '|' indicating the new periodic length, within which the occupational modulation function is commensurate with the orthorhombic

unit cell of the average structure, cf. Fig. 9b).[3] This leads to a changed Ni(2) content of $\delta = 6/14 = 0.429$. Since there are three periods λ on $7a_{\mathrm{orth}}$ one gets $|\mathbf{q}| = q = 1/\lambda = 3/7a^*_{\mathrm{orth}} = 0.429a^*_{\mathrm{orth}}$. More general, if n_1 rows '0' are added to n_2 initial 1100 cells, one obtains $\delta = 2/(4 + n_1/n_2)$. Then, the wavelength λ of the resulting modulation wave corresponds to the average length of the basic 1100(0) unit in terms of a_{orth}, $\lambda = (4 + n_1/n_2)a_{\mathrm{orth}}/2$ ($n_1 = 0$ gives $\lambda = 2a_{\mathrm{orth}}$). By this, the length of the modulation vector q corresponds to $q = 1/\lambda = 2/(a_{\mathrm{orth}}(4 + n_1/n_2)) = \delta a^*_{\mathrm{orth}}$ or $\alpha = \delta$. The same also holds for q when a certain amount of '0' rows are removed, e.g., for $Ni_{1.600}Sn$ (Fig. 9c). The layers at $z = 3/4$ can be constructed from those at $z = 1/4$ by application of the *.n.* glide plane operation.

In order to compare this model with reality, the function $\alpha(\delta) = \delta$ is plotted in Fig. 10 together with the experimental values. A first difference between the model and reality is the plateau in $\alpha(\delta)$ in the composition range of the LT phase. Here, α is 'locked' [29] at a value 1/2 as expected for a commensurate phase, whereas α varies continuously with δ in the LT′ phase. However, secondly, the model does not quantitatively describe the slope of $\alpha(\delta)$ for the LT′ phase (compare Fig. 3). The average slope of $d\alpha(\delta)/d\delta$ is closer to 1/2 than to 1. Nevertheless, the model may give ideas about the main tendencies for $\alpha(\delta)$.

For $\alpha = \delta = 0.5$ this idealized model corresponds to the LT-$Ni_{1.50}Sn$ phase. Furthermore, the $Ni_{1.600}Sn$ structure ($\alpha = \delta = 0.6$) corresponds to the commensurate approximant derived for $Mn_{1.62}Sn$ (Mn_8Sn_5, [13]). This phase is actually incommensurate and has the *Cmcm*(α00)0*s*0 symmetry as LT′ with $\mathbf{q} = 0.616 \cdot \mathbf{a}^*_{\mathrm{orth}}$. The occupational modulation of Mn has successfully been described in Ref. [13] by a *Crenel* function, and is, therefore, well ordered in contrast to the LT′-$Ni_{1+\delta}Sn$ phase. An analysis of the dominant displacive modulation functions of Sn confirms that $Mn_{1.62}Sn$ in fact shows strong similarities with the LT′ and LT phases.

5. Conclusions

1. Detailed investigations of the crystal structures of LT′- ($\delta = 0.35$, 0.38, 0.41) and LT-$Ni_{1+\delta}Sn$ ($\delta = 0.47$ and 0.50) by Rietveld refinement revealed besides the occupational modulations of Ni(2) considerable atomic displacements, especially of Sn. These, and also lattice distortions relative to the HT phase, can be explained by an adaptation of the overall atomic arrangement to the occupational order of Ni(2).
2. There are close analogies between the crystal structures of the commensurate LT phase and the incommensurate LT′ phase, which can be explained by a common idealized structure model describing the ordering of Ni(2). The LT phase is a lock-in phase of the LT′ phase.
3. In the LT′ phase, there is an appreciable disordering of the structure below the transition temperature as indicated by the variation of the order parameters as a function of the annealing temperature.

[3] The model structures considered here are only those, which have an even number of rows in the new periodic length of the sequence, because a unit cell of the average structure contains two rows.

Acknowledgments

The author wishes to thank Dr. V. Petricek for helpful discussions concerning the Rietveld options of Jana2000 and incommensurate structures in general, and Prof. Dr. E.J. Mittemeijer for his support and interest in the work.

References

[1] P. Nash, A. Nash, Bull. Alloy Phase Diagr. 6 (1985) 350.
[2] S. Lidin, Acta Crystallogr. B 54 (1998) 97.
[3] S. Lidin, A.-K. Larsson, J. Solid State Chem. 118 (1995) 313.
[4] H. Fjellvåg, A. Kjekshus, Acta Chem. Scand. A 40 (1986) 23.
[5] M. Ellner, J. Less-Common Met. 48 (1976) 21.
[6] P. Brand, Z. Anorg. Allg. Chem. 353 (1967) 270.
[7] A. Leineweber, M. Ellner, E.J. Mittemeijer, J. Solid State Chem. 159 (2001) 191.
[8] H.W. King, Bull. Alloy Phase Diagr. 2 (1981) 402.
[9] E.J. Sonneveld, R. Delhez, ProFit, Version 1.0c, Phillips Electronics N.V., 1996.
[10] K. Koths, ASIN, Version 7.4 (1987), Based on a code by F. Stewner (1970).
[11] M. Dušek, V. Petricek, M. Wunschel, R.E. Dinnebier, S. van Smaalen, J. Appl. Crystallogr. 34 (2001) 398.
[12] P. Thompson, D.E. Cox, J.B. Hastings, J. Appl. Crystallogr. 20 (1987) 79.
[13] M. Elding-Pontén, L. Stenberg, S. Lidin, G. Madariaga, J.-M. Pérez Mato, Acta Crystallogr. B 53 (1997) 364.
[14] V. Petricek, V. van der Lee, M. Evain, Acta Crystallogr. A: Found. Crystallogr. 51 (1995) 529.
[15] J.M. Perez-Mato, G. Madariaga, F.J. Zuñiga, A. Garcia Arribas, Acta Crystallogr. A: Found. Crystallogr. 43 (1987) 216.
[16] J.M. Pérez-Mato, in: J.M. Pérez-Mato, F.J. Zúniga, G. Madariaga (Eds.), Methods of Structural Analysis of Modulated Structures and Quasicrystals, World Scientific, Singapore, p. 117.
[17] S. van Smaalen, Acta Crystallogr. A: Found. Crystallogr. 43 (1987) 202.
[18] Ph. Sciau, D. Grebille, Phys. Rev. B 39 (1989) 11982.
[19] P. Brand, Z. Anorg. Allg. Chem. 358 (1968) 170.
[20] H. Bärninghausen, MATCH 9 (1980) 139.
[21] E. Teatum, K. Gschneidner, J. Waber, Compilation of calculated data useful in predicting metallurgical behaviour of the elements in binary alloy systems, LA-2345, Los Alamos Scientific Laboratory, 1960.
[22] L.P. Komarovskaya, L.G. Aksel'rud, R.V. Skolozdra, Kristallografia 28 (1983) 1201.
[23] A.-K. Larsson, R.L. Withers, L. Stenberg, J. Solid State Chem. 127 (1996) 222.

[24] A. Leineweber, E.J. Mittemeijer, O. Oeckler, U. Zachwieja, J. Solid State Chem., in press.
[25] A.K. Larsson, L. Stenberg, S. Lidin, Acta Crystallogr. B: Struct. Sci. 50 (1994) 636.
[26] A.K. Larsson, L. Stenberg, S. Lidin, Z. Kristallogr. 210 (1995) 832.
[27] M. Stange, H. Fjellvåg, S. Furuseth, B.C. Hauback, J. Alloys Compd. 259 (1997) 140.
[28] K.C. Jain, M. Ellner, K. Schubert, Z. Metallkd. 63 (1972) 258.
[29] F. Ducastelle, Order and Phase stability in Alloys, North-Holland, Amsterdam, 1991.